Monthly Notices
of the
ROYAL ASTRONOMICAL SOCIETY

MNRAS **460,** L84–L88 (2016)
Advance Access publication 2016 April 28

doi:10.1093/mnrasl/slw082

# A shock at the radio relic position in Abell 115

A. Botteon,[1,2]★ F. Gastaldello,[3] G. Brunetti[2] and D. Dallacasa[1,2]

[1]*Dipartimento di Fisica e Astronomia, Università di Bologna, via C. Ranzani 1, I-40127 Bologna, Italy*
[2]*INAF – ORA, via P. Gobetti 101, I-40129 Bologna, Italy*
[3]*INAF – IASF Milano, via E. Bassini 15, I-20133 Milano, Italy*

Accepted 2016 April 23. Received 2016 April 14; in original form 2016 March 15

## ABSTRACT

We analysed a deep *Chandra* observation (334 ks) of the galaxy cluster Abell 115 and detected a shock cospatial with the radio relic. The X-ray surface brightness profile across the shock region presents a discontinuity, corresponding to a density compression factor $\mathcal{C} = 2.0 \pm 0.1$, leading to a Mach number $\mathcal{M} = 1.7 \pm 0.1$ ($\mathcal{M} = 1.4{-}2$ including systematics). Temperatures measured in the upstream and downstream regions are consistent with what expected for such a shock: $T_{\rm u} = 4.3^{+1.0}_{-0.6}$ keV and $T_{\rm d} = 7.9^{+1.4}_{-1.1}$ keV, respectively, implying a Mach number $\mathcal{M} = 1.8^{+0.5}_{-0.4}$. So far, only few other shocks discovered in galaxy clusters are consistently detected from both density and temperature jumps. The spatial coincidence between this discontinuity and the radio relic edge strongly supports the view that shocks play a crucial role in powering these synchrotron sources. We suggest that the relic is originated by shock re-acceleration of relativistic electrons rather than acceleration from the thermal pool. The position and curvature of the shock and the associated relic are consistent with an off-axis merger with unequal mass ratio where the shock is expected to bend around the core of the less massive cluster.

**Key words:** radiation mechanisms: non-thermal – shock waves – galaxies: clusters: individual: A115 – radio continuum: general – X-rays: galaxies: clusters.

## 1 INTRODUCTION

Galaxy clusters hierarchically form by the aggregation of smaller structures. In the process of cluster formation, shocks and turbulence are produced in the intra-cluster medium (ICM) and dissipate a significant fraction of kinetic energy. A fraction of the dissipated energy can also be channelized into non-thermal components, such as magnetic fields and relativistic particles (e.g. Brunetti & Jones 2014, for a review).

Shock waves are detectable in the X-rays and appear as sharp surface brightness discontinuities related to a temperature increase in the downstream region. However, shocks in galaxy clusters are difficult to detect because projections effects could hide temperature and density jumps and because the strongest shocks are expected in the clusters outskirts, where the X-ray brightness is low. For this reason, only few of them have been clearly detected, i.e. showing both surface brightness and temperature jumps (e.g. Markevitch et al. 2002, 2005; Russell et al. 2010; Macario et al. 2011; Dasadia et al. 2016).

There is a broad consensus that shocks play an important role in the (re)acceleration of radio-emitting electrons generating radio relics (see Brüggen et al. 2012; Brunetti & Jones 2014, for reviews). In general, radio relics are polarized synchrotron sources found in the periphery of a number of galaxy clusters (e.g. Feretti et al. 2012, for an observational overview). They have arc-shaped morphologies and, in some cases, their connection with shocks waves is directly established by X-ray observations (e.g. Macario et al. 2011; Akamatsu & Kawahara 2013; Bourdin et al. 2013).

Abell 115 (hereafter A115) is an X-ray luminous ($L_{\rm X} = 1.5 \times 10^{45}$ erg s$^{-1}$ in the 0.1–2.4 keV band) and dynamically disturbed cluster at $z = 0.197$. Early X-rays observations (Forman et al. 1981; Shibata et al. 1999) revealed that A115 has an X-ray brightness distribution characterized by two peaks, the brightest one being in the north region and roughly coincident with the position of the radio galaxy 3C28. More recently, *Chandra* observations (Gutierrez & Krawczynski 2005) suggested that A115 is undergoing an off-axis merger, while optical studies confirmed the presence of two subclusters in a merging state (Barrena et al. 2007). In the radio band, A115 exhibits a giant radio relic at the edge of the northern part of the cluster that extends for ∼1.5 Mpc (Govoni et al. 2001).

In this Letter, we report the discovery of a shock associated with the radio relic from the analysis of *Chandra* and Very Large Array (VLA) observations of A115. Hereafter, we assume a concordance Λcold dark matter cosmology with $H_0 = 70$ km s$^{-1}$ Mpc$^{-1}$, $\Omega_{\rm m} = 0.3$ and $\Omega_\Lambda = 0.7$. At the redshift of A115 ($z = 0.197$), the luminosity distance is 673 Mpc and 1 arcsec corresponds to 3.261 kpc. Reported uncertainties are 68 per cent, unless stated otherwise.

★E-mail: botteon@ira.inaf.it

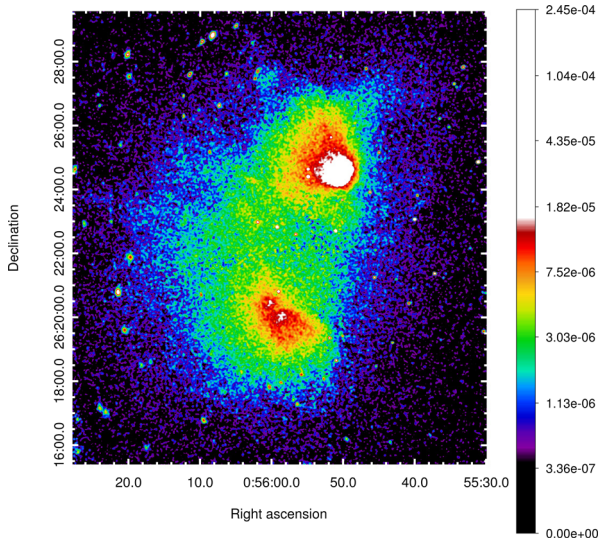


**Figure 1.** *Chandra* exposure-corrected image in the 0.5–2 keV band of A115. The image is smoothed on a 3 arcsec scale. The colourbar is in logarithmic scale, units are count $s^{-1}$.

## 2 OBSERVATIONS AND DATA REDUCTION

### 2.1 X-ray data reduction

We analysed the *Chandra* ACIS-I observations of A115 in `VFAINT` mode (ObsID: 3233, 13458, 13459, 15578, 15581) with CIAO 4.7 and *Chandra* CALDB 4.6.9. All data were reprocessed from `level=1` event file following the standard *Chandra* reduction threads. For the observations in which the S3 chip was active (ObsID: 3233, 13459, 15581), we extracted light curves from this chip in the 0.5–2 keV band and we cleaned from soft proton flares using the `deflare` task with the `clean=yes` option. For the other ObsIDs, light curves were instead extracted from a cluster free emission region in one ACIS-I chip. We combined the observations with the `merge_obs` script and produced the 0.5–2 keV image binned by a factor of 2, shown in Fig. 1. The total cleaned exposure time of this image is 334 ks.

For each observation, we created a point spread function (PSF) map at 1.5 keV. These were combined with the corresponding exposure maps in order to obtain a single exposure-corrected PSF map with minimum size. We then ran the `wavdetect` task on the merged image in order to detect point sources. Sources were visually confirmed and then excluded in the further analysis. We used the task `reproject_event` to match background templates to the corresponding event files for every ObsID. Then they were normalized by counts in the 9.5–12 keV energy band and combined in a single background image subtracted in the surface brightness analysis.

Spectral extraction was performed for every ObsID using the same regions. We modelled the particle background following Bartalucci et al. (2014) and the sky component with two thermal plasmas at temperatures of 0.14 and 0.25 keV to account for the Galactic emission and an absorbed power law with photon index $\Gamma = 1.4$ to account for the cosmic X-ray background. The background parameters were determined by fitting spectra extracted from cluster-free emission regions at the edge of the field of view in the 0.5–11 keV energy band. The cluster emission was fitted with a thermal model with metal abundance fixed at 0.3 $Z_{\odot}$. All fits were performed using Cash statistics. The robustness of the fits was verified by checking for systematic errors due to the background determination. For this reason, we re-performed the cluster spectral analysis with the background normalization levels fixed at $\pm 1\sigma$ within their best-fitting values. In addition, the impact of ACIS quantum efficiency contamination at low energy was verified by fitting in the bands 0.5–11 and 1–11 keV. In both cases, the thermal parameters of the fits are consistent within $1\sigma$.

### 2.2 Radio data reduction

We reanalysed VLA archival data at 1.4 GHz in the C and D configurations. Details of observations can be found in Govoni et al. (2001). The two data sets were edited, calibrated and imaged separately. Particular care was devoted to the identification and removal of bad data corrupted by intermittent radio frequency interference. After a number of phase only self-calibration iterations and an accurate comparison of the flux densities of the sources, the data of IF1, at 1364 MHz for both data sets, were combined (the second IF could not be used given the significantly different frequency).

The final data set (4.5 h and $\Delta\nu = 50$ MHz) was once again self-calibrated a number of times and final images were obtained using different weighting schemes. The image shown in Fig. 2(a) was made with a two-scale clean where the extended emission was deconvolved using a larger beam (∼30 arcsec). The restoring beam is 15 arcsec × 14 arcsec in position angle −35° and the off-source noise level is 70 μJy $b^{-1}$. Errors on flux densities are dominated by the 5 per cent uncertainty of the absolute flux scale calibration.

## 3 RESULTS

A visual inspection of the X-ray image of A115 led us to identify a surface brightness jump in the northern part of the system, cospatially located with the relic position (Fig. 2). The surface brightness profile was extracted in the red sector shown in Fig. 2(b) and fitted with PROFFIT v1.3 (Eckert, Molendi & Paltani 2011). The data were fitted assuming an underlying broken power-law density profile in the form

$$\begin{aligned} n_d(r) &= \mathcal{C} n_0 \left(\tfrac{r}{r_{sh}}\right)^{a_1}, \quad \text{if} \quad r \leq r_{sh}, \\ n_{\rm u}(r) &= n_0 \left(\tfrac{r}{r_{\rm sh}}\right)^{a_2}, \quad \text{if} \quad r > r_{\rm sh}, \end{aligned} \tag{1}$$

where $\mathcal{C} \equiv n_{\rm d}/n_{\rm u}$ is the compression factor of the shock, $n_0$ is the density normalization, $a_1$ and $a_2$ are the power-law indices, $r$ is the radius from the centre of the sector and $r_{\rm sh}$ is the radius corresponding to the putative shock front (which curvature relative to the line of sight is assumed to be the same as that in the plane of the sky). Subscripts $u$ and $d$ indicate quantities upstream and downstream of the shock, respectively. All the parameters of the model were let free in the fit. The best-fitting broken power law is shown in Fig. 3. The compression factor taken from the red sector in Fig. 2(b) is $\mathcal{C} = 2.0 \pm 0.1$. By using an adiabatic index $\gamma = 5/3$ and the Rankine–Hugoniot jump conditions, this leads to a Mach number $\mathcal{M} = 1.7 \pm 0.1$. Obviously, this value does not include systematics deriving from 3D model geometry and the shape of the extraction region. We explored uncertainties due to the sector choice by varying its curvature radius, aperture and position angle. Tests were made keeping the discontinuity distance frozen. Changing the shock curvature radius from its best value 360 kpc by a factor of 0.5 and 1.5 gives the highest variation in terms of the compression factor, 1.6–2.1, corresponding to $\mathcal{M} = 1.4-1.8$. Varying the other parameters of the region results in values of $\mathcal{M}$ within this range.

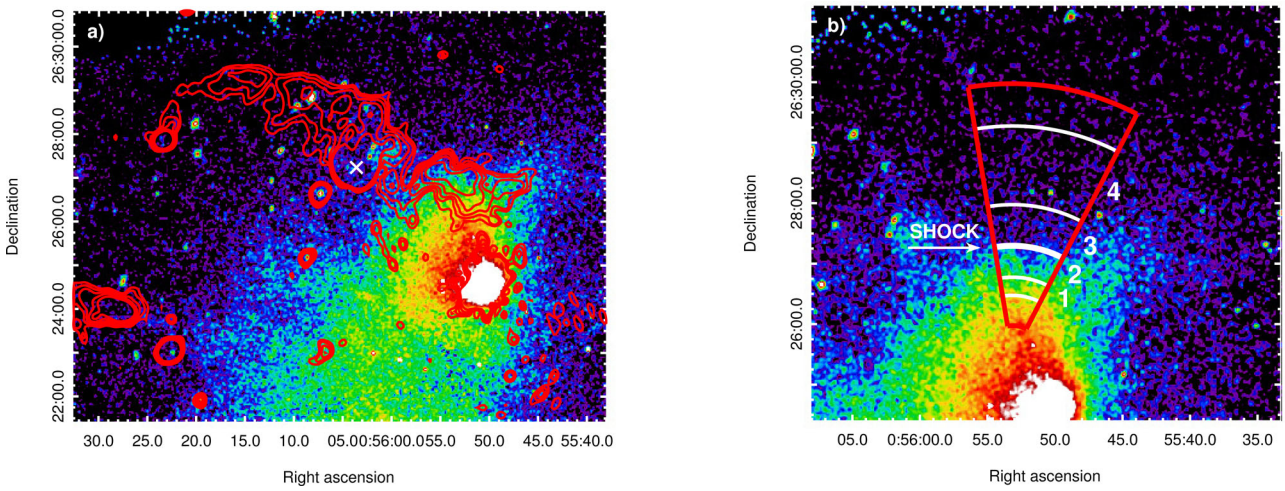


**Figure 2.** Zoom on the northern region of A115. (*a*) Radio contours at 1.4 GHz of the relic source in A115. The resolution is 15 arcsec × 14 arcsec. Contour levels are $0.21 \times \pm(\sqrt{2})^n$ mJy b$^{-1}$, with $n = 1, 2, 3, 4$. The $1\sigma$ noise level is 70 μJy b$^{-1}$. White cross denotes the 0056 + 26 B radio galaxy. (*b*) Red sector delineates the region where the X-ray surface brightness profile was extracted; white sectors represent the four bins where spectral analysis was performed. In both panels, colours represent the *Chandra* image (same as Fig. 1).

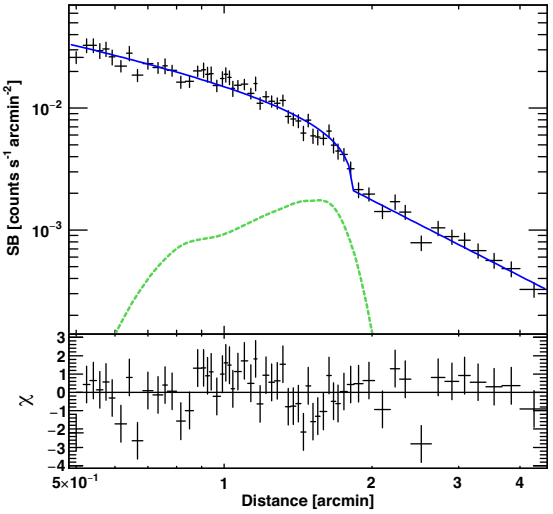


**Figure 3.** X-ray surface brightness profile in the 0.5–2 keV band extracted in the red region shown in Fig. 2(b). The data were rebinned to reach a minimum signal-to-noise ratio of 7. The fit had $\chi^2$/dof = 1.2. The green dashed line shows the radio relic brightness profile (in arbitrary units).

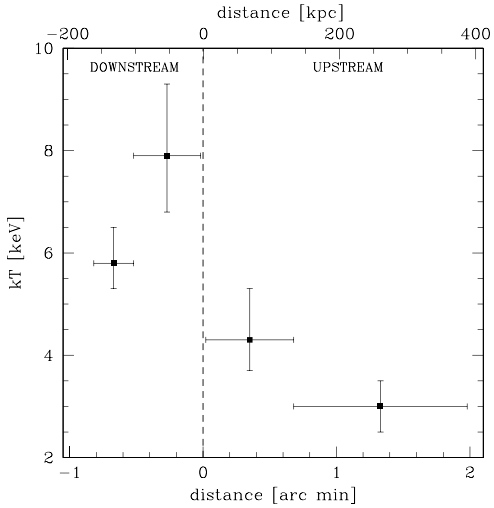


**Figure 4.** Temperature profile across the shock. The vertical dashed line sets the location of the X-ray surface brightness discontinuity.

We did not introduce any ellipticity in the problem as the surface brightness edge looks quite straight. The red sector in Fig. 2(b) represents the best compromise to highlight the discontinuity in terms of $\chi^2$/dof.

In a shock wave, the downstream region is characterized by a temperature increase; in a cold front, instead, the denser region has a lower temperature (see e.g. Markevitch & Vikhlinin 2007). For this reason, we extracted spectra in the four white regions shown in Fig. 2(b) and performed spectral fitting. We found a temperature jump from $T_u = 4.3^{+1.0}_{-0.6}$ keV to $T_d = 7.9^{+1.4}_{-1.1}$ keV in the two bins closer to the surface brightness discontinuity, confirming the shock nature of this feature. This temperature jump corresponds to $\mathcal{M} = 1.8^{+0.5}_{-0.4}$, in agreement with the Mach number derived from the density jump; projection effects, if they play a role, are expected to make the intrinsic jump slightly smaller. The temperature profile taken across the shock region is shown in Fig. 4. The first bin exhibits a low temperature, this could either be the result of the gas expansion behind the shock or the presence of a substructure along the line of sight (e.g. Markevitch et al. 2002). For a sanity check, we re-performed the surface brightness fit avoiding this temperature bin by excluding data points at $r < 1.5$ arcmin; in this case, we achieve $\mathcal{C} = 2.0 \pm 0.3$, leading to $\mathcal{M} = 1.7^{+0.3}_{-0.2}$.

## 4 DISCUSSION

### 4.1 Radio relic–shock connection

At the resolution of 15 arcsec × 14 arcsec, the radio relic in A115 presents a discontinuity in the centre of its northern edge structure, roughly splitting it in two parts (Fig. 2a). One is quite short, straight in the E–W direction and coincides with the shock location, while the remainder extends in the eastern direction beyond the cluster X-ray emission and appears slightly bent. Given the spatial coincidence with the shock, we suggest that the former is a 'classical'

radio relic where particles are accelerated or re-accelerated by the passage of the shock. In this restricted region, the radio flux density at 1.4 GHz is $F = 34 \pm 2$ mJy. The eastern radio emission is more difficult to interpret and it could be produced by the uplifting of the plasma coming from the cluster radio bright source 0056 + 26 B (a narrow angle tailed radio galaxy whose emission fades away in the east direction), located in the middle of the relic, after the shock passage.

In a case of a head-on merging in the plane of the sky between two clusters with similar mass, radio relics are expected to come in pairs in opposite directions along the axis merger (e.g. Röttgering et al. 1997). This is clearly not the case of A115 where the relic has an unusual location as it is oriented almost parallel to the northern subcluster motion. This led to doubts about the nature of relic-extended emission and to the interpretation as tails of radio plasma trailing the radio galaxies (Gutierrez & Krawczynski 2005). However, numerical simulations of an off-axis merger between clusters with different mass predicts that the shock curves around the core of the minor cluster (see fig. 7 in Ricker & Sarazin 2001), in agreement with A115-N subcluster being less massive (Barrena et al. 2007).

### 4.2 Acceleration efficiency

There is consensus on the hypothesis that shocks play an important role for the origin of radio relics. However, the case of shock acceleration of cosmic ray electrons (CRe) from the thermal ICM is challenged by the large efficiencies that are required to reproduce the total radio luminosity of several relics (Brunetti & Jones 2014, for review). Large acceleration efficiencies would also lead to a cosmic ray protons (CRp) induced $\gamma$-ray emission exceeding current clusters upper limits in the case that shocks in the ICM produce a ratio CRp/CRe similar to that in supernova remnants (Vazza & Brüggen 2014). To alleviate the large requirements for acceleration efficiencies of CRe, recent models for cluster relics assume shock re-acceleration of a pre-existing population of CRe (Markevitch et al. 2005; Kang, Ryu & Jones 2012; Pinzke, Oh & Pfrommer 2013; Kang et al. 2014).

A115 is a test case to constrain the origin of the shock–relic connection, because the underlying shock is well constrained. If the downstream synchrotron luminosity emitted at frequency $\geq\nu_0$ originates from electrons in steady state conditions, the bolometric ($\geq\nu_0$) synchrotron luminosity that is generated via shock acceleration from a shock with speed $V_{\rm sh}$, surface $S$ and upstream mass density $\rho_{\rm u}$ can be estimated as

$$\int_{\nu_0} L(\nu)\,{\rm d}\nu \simeq \frac{1}{2}\eta_{\rm e}\Psi\rho_{\rm u}V_{\rm sh}^3\left(1-\frac{1}{\mathcal{C}^2}\right)\frac{B^2}{B_{\rm cmb}^2+B^2}S, \quad (2)$$

where $\eta_{\rm e}$ is the efficiency of electron acceleration,

$$\Psi = \frac{\int_{p_{\rm min}} Q(p)E\,{\rm d}p}{\int_{p_0} Q(p)E\,{\rm d}p}, \quad (3)$$

accounts for the ratio of the energy flux injected in 'all' electrons and those visible in the radio band ($\nu \geq \nu_0$), $p_0$ is the momentum of the relativistic electrons emitting the synchrotron frequency $\nu_0$ in a magnetic field $B$ and $B_{\rm cmb} = 3.25(1+z)^2$ μG accounts for inverse Compton scattering of cosmic microwave background photons.

A model of shock acceleration from the thermal pool, for the relic, is readily rule out by our measurements. According to diffusive shock acceleration theory, the particles injection spectrum is $Q(p) \propto p^{-\delta_{\rm inj}}$ with $\delta_{\rm inj} = 2(\mathcal{M}^2+1)/(\mathcal{M}^2-1)$ (e.g. Blandford & Eichler 1987), that for $\mathcal{M} = 1.7-1.8$ would imply $\delta_{\rm inj} = 4$–$3.8$ (and integrated spectral index $\alpha = \delta_{\rm inj}/2 = 2$–$1.9$). Not only this is inconsistent with the measured spectrum of the relic ($\alpha \sim 1.1$; Govoni et al. 2001), but from equation (2), it also requires an untenable large acceleration efficiency (assuming $S = \pi \times 180 \times 180\,{\rm kpc}^2$).

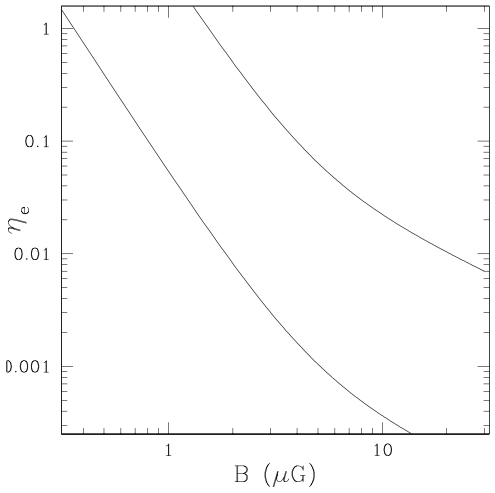


**Figure 5.** Electron acceleration efficiency versus magnetic field downstream in the shock in A115. Lines represent efficiencies evaluated for re-accelerated electrons with $p_{\rm min}/m_{\rm e}c = 20$ (top) and 200 (bottom) and $\delta_{\rm inj} = 3.8$.

Alternatively, we can assume re-acceleration. In this case, the initial (upstream) and accelerated spectra of electrons are connected via

$$N_{\rm d}(p) = (\delta_{\rm inj}+2)p^{-\delta_{\rm inj}}\int_{p_{\rm min}}^{p} x^{\delta_{\rm inj}-1}N_{\rm u}(x)\,{\rm d}x, \quad (4)$$

where $N_{\rm u}$ refers to the upstream spectrum of seed particles; re-acceleration efficiencies can be larger compared to the case of acceleration from thermal ICM, because seed ultrarelativistic electrons diffuse efficiently across the shock discontinuity (e.g. Brunetti & Jones 2014). In Fig. 5, we show the case of a spectrum of re-accelerated electrons with power law $\delta_{\rm inj} = 3.8$ and $p_{\rm min}/m_{\rm e}c = 20$ and 200. Re-acceleration of electrons with $p_{\rm min} \geq 100\,m_{\rm e}c$ appears energetically viable. In this case, however, the spectrum of the relic would be very steep ($\alpha \sim 2$). Alternatively, the shock may re-accelerate a cloud of electrons that are not very old and have a flatter spectrum. In this case, the shock essentially boosts their emission at higher frequencies preserving the seed spectrum (equation 4; see e.g. Kang & Ryu 2016, for details). As already discussed in Section 4.1, re-acceleration is also suggested by the morphology of the radio relic and by the fact that the relic embeds a few radio galaxies that would be natural sources of seed particles. Finally, we note that the eastern part of the radio relic deploys in a region of low-X-ray surface brightness where the thermal energy density is small and where a scenario of shock acceleration of thermal electrons would require an efficiency that is even larger than that shown in Fig. 5.

## 5 CONCLUSIONS

We presented results concerning the merging galaxy cluster A115 at $z = 0.197$. We analysed a *Chandra* data set for a total exposure time of 334 ks and archival VLA radio observations at 1.4 GHz. In this Letter, we focused on A115-N, where a giant radio relic stands out.

The deep *Chandra* observations led us to detect a shock spatially coincident with the radio relic in A115. Assuming a broken power-law density profile, the surface brightness discontinuity is consistent with a density compression factor $\mathcal{C} = 2.0 \pm 0.1$, which in turn results in $\mathcal{M} = 1.7 \pm 0.1$; the Mach number is in the range 1.4–2, including systematic uncertainties. The shock nature of the discontinuity was confirmed by spectral analysis of the downstream and the upstream regions, where a temperature jump from $T_{\rm d} = 7.9^{+1.4}_{-1.1}$ keV to $T_{\rm u} = 4.3^{+1.0}_{-0.6}$ keV was found, implying $\mathcal{M} = 1.8^{+0.5}_{-0.4}$. This is one of the few cases where the surface brightness and temperature drops in a merger shock are clearly detected and are in excellent agreement.

In the radio band, the relic can be roughly divided into a W and an E part. The former is a 'classical' relic spatially coincident with the shock found in the X-rays. The relic location is in agreement with an off-axis merger between two clusters with unequal mass, where the shock bends around the core of the less massive system. The eastern relic radio emission is harder to interpret as, in this region, a proper X-ray analysis cannot be performed, given its low surface brightness. An attractive scenario is the uplifting of the cluster radio galaxy 0056 + 26 B plasma after the shock sweeping in the cluster outskirts.

Confirming the presence of a shock underlying a radio relic strongly supports the scenario where radio relics are powered by emitting particles produced during merger shocks. Given the low Mach number, spectrum and morphology of the relic, models in which relativistic seed electrons are re-accelerated by the shock passage are favoured. In this respect, the few cluster radio galaxies embedded in the relic in A115 could naturally provide the required seed particles.

## ACKNOWLEDGEMENTS

We thank the anonymous referee for the useful comments on the manuscript. We are grateful to Dominique Eckert for developing and making available a powerful tool such as PROFFIT. The scientific results reported in this Letter are based on observations made by the *Chandra X-ray Observatory*. The NRAO is a facility of the National Science Foundation operated under cooperative agreement by Associated Universities, Inc. AB and GB acknowledge partial support from PRIN-INAF 2014. GB acknowledges partial support from von Humboldt Foundation. FG acknowledges financial support from PRIN-INAF 2012 and ASI-INAF I/037/12/0.

## REFERENCES

Akamatsu H., Kawahara H., 2013, PASJ, 65, 16
Barrena R., Boschin W., Girardi M., Spolaor M., 2007, A&A, 469, 861
Bartalucci I., Mazzotta P., Bourdin H., Vikhlinin A., 2014, A&A, 566, A25
Blandford R., Eichler D., 1987, Phys. Rep., 154, 1
Bourdin H., Mazzotta P., Markevitch M., Giacintucci S., Brunetti G., 2013, ApJ, 764, 82
Brüggen M., Bykov A., Ryu D., Röttgering H., 2012, Space Sci. Rev., 166, 187
Brunetti G., Jones T., 2014, Int. J. Mod. Phys. D, 23, 30007
Dasadia S. et al., 2016, ApJ, 820, L20
Eckert D., Molendi S., Paltani S., 2011, A&A, 526, A79
Feretti L., Giovannini G., Govoni F., Murgia M., 2012, A&AR, 20, 54
Forman W., Bechtold J., Blair W., Giacconi R., van Speybroeck L., Jones C., 1981, ApJ, 243, L133
Govoni F., Feretti L., Giovannini G., Böhringer H., Reiprich T. H., Murgia M., 2001, A&A, 376, 803
Gutierrez K., Krawczynski H., 2005, ApJ, 619, 161
Kang H., Ryu D., 2016, preprint (arXiv:1602.03278)
Kang H., Ryu D., Jones T., 2012, ApJ, 756, 97
Kang H., Petrosian V., Ryu D., Jones T., 2014, ApJ, 788, 142
Macario G., Markevitch M., Giacintucci S., Brunetti G., Venturi T., Murray S., 2011, ApJ, 728, 82
Markevitch M., Vikhlinin A., 2007, Phys. Rep., 443, 1
Markevitch M., Gonzalez A., David L., Vikhlinin A., Murray S., Forman W., Jones C., Tucker W., 2002, ApJ, 567, L27
Markevitch M., Govoni F., Brunetti G., Jerius D., 2005, ApJ, 627, 733
Pinzke A., Oh S., Pfrommer C., 2013, MNRAS, 435, 1061
Ricker P., Sarazin C., 2001, ApJ, 561, 621
Röttgering H., Wieringa M., Hunstead R., Ekers R., 1997, MNRAS, 290, 577
Russell H., Sanders J., Fabian A., Baum S., Donahue M., Edge A., McNamara B., O'Dea C., 2010, MNRAS, 406, 1721
Shibata R., Honda H., Ishida M., Ohashi T., Yamashita K., 1999, ApJ, 524, 603
Vazza F., Brüggen M., 2014, MNRAS, 437, 2291

This paper has been typeset from a TEX/LATEX file prepared by the author.